9078 *Biochemistry* **2010,** *49,* 9078–9088
DOI: 10.1021/bi1007222

BIOCHEMISTRY
including biophysical chemistry & molecular biology
Article

The Tail Wagging the Dog: Insights into Catalysis in R67 Dihydrofolate Reductase[†]

Ganesh Kamath,[‡] Elizabeth E. Howell,[§] and Pratul K. Agarwal*[,‡]

[‡]*Computer Science and Mathematics Division, Oak Ridge National Laboratory, Oak Ridge, Tennessee 37831, and* [§]*Department of Biochemistry and Cellular and Molecular Biology, University of Tennessee, Knoxville, Tennessee 37996*

Received May 6, 2010; Revised Manuscript Received August 26, 2010

ABSTRACT: Plasmid-encoded R67 dihydrofolate reductase (DHFR) catalyzes a hydride transfer reaction between substrate dihydrofolate (DHF) and its cofactor, nicotinamide adenine dinucleotide phosphate (NADPH). R67 DHFR is a homotetramer that exhibits numerous characteristics of a primitive enzyme, including promiscuity in binding of substrate and cofactor, formation of nonproductive complexes, and the absence of a conserved acid in its active site. Furthermore, R67's active site is a pore, which is mostly accessible by bulk solvent. This study uses a computational approach to characterize the mechanism of hydride transfer. Not surprisingly, NADPH remains fixed in one-half of the active site pore using numerous interactions with R67. Also, stacking between the nicotinamide ring of the cofactor and the pteridine ring of the substrate, DHF, at the hourglass center of the pore, holds the reactants in place. However, large movements of the *p*-aminobenzoylglutamate tail of DHF occur in the other half of the pore because of ion pair switching between symmetry-related K32 residues from two subunits. This computational result is supported by experimental results that the loss of these ion pair interactions (located >13 Å from the center of the pore) by addition of salt or in asymmetric K32M mutants leads to altered enzyme kinetics [Hicks, S. N., et al. (2003) *Biochemistry 42*, 10569−10578; Hicks, S. N., et al. (2004) *J. Biol. Chem. 279*, 46995−47002]. The tail movement at the edge of the active site, coupled with the fixed position of the pteridine ring in the center of the pore, leads to puckering of the pteridine ring and promotes formation of the transition state. Flexibility coupled to R67 function is unusual as it contrasts with the paradigm that enzymes use increased rigidity to facilitate attainment of their transition states. A comparison with chromosomal DHFR indicates a number of similarities, including puckering of the nicotinamide ring and changes in the DHF tail angle, accomplished by different elements of the dissimilar protein folds.

R-Plasmid-encoded dihydrofolate reductase (R67 DHFR)[1] catalyzes the reduction of dihydrofolate (DHF) to tetrahydrofolate (THF) using nicotinamide adenine dinucleotide phosphate (NADPH) as a cofactor. While the reaction is the same as that catalyzed by the chromosomally encoded DHFR in *Escherichia coli* (EcDHFR) and other organisms, R67 shows neither sequence nor structural homology with chromosomal DHFRs (*1*−*4*). This type II DHFR was discovered because of its ability to confer trimethoprim resistance upon host bacteria (*5*). Each R67 DHFR monomer is 78 amino acids long, and the subunits assemble into a homotetramer possessing 222 symmetry (see Figure 1). A single active site pore with a volume of 3626 Å^3 traverses the length of the molecule. R67 DHFR possesses a SH3 domain-like fold, while EcDHFR displays a Rossmann fold, the latter being a characteristic feature of dinucleotide binding proteins (*6*). R67 is an unusual enzyme as it uses symmetry-related sites to bind various combinations of ligands, including two substrate (DHF) molecules or two cofactor (NADPH) molecules or the catalytically relevant combination of one DHF molecule and one NADPH molecule (*7*).

R67 DHFR has been described as a primitive enzyme because of several features, including an unusual active site pore that is mostly accessible by bulk water except at the hourglass center, no conserved acid or base in the pore, formation of nonproductive 2DHF or 2NADPH complexes, and a low catalytic efficiency ($\sim 3 \times 10^5$ s^{-1} M^{-1}) compared to that of EcDHFR (*1*). Moreover, this enzyme behaves in a manner different from the conventional paradigm of enzyme catalysis in a number of ways. First, the binding-site promiscuity for different ligands in R67 deviates from the lock-and-key hypothesis, as DHF and NADPH share symmetry-related sites; α-NADPH can be used as cofactor (*8*), and novobiocin and congo red are inhibitors [with K_i values of 70 and 2 μM, respectively (*9*, *10*)]. Neither of the latter two ligands resembles the substrate and/or the cofactor. Second, a widely accepted view of enzyme catalysis suggests that an increase in rigidity in the active site or enthalpy driven binding of the transition state facilitates catalysis (*11*−*15*). In other words, loss of translational and rotational motion in a well-evolved active site leads to the correct positioning of enzyme and reactants, thus facilitating the chemical step of the reaction.

[†]The contributions of G.K. and P.K.A. were supported by Oak Ridge National Laboratory's Laboratory Directed Research and Development funds and the allocation of computing time by the National Center for Computational Sciences (BIP003). The contribution of E.E.H. was supported by National Science Foundation Grant MCB-0817827.

*To whom correspondence should be addressed: Oak Ridge National Laboratory, P.O. Box 2008, MS 6016, Oak Ridge, TN 37831. Phone: (865) 574-7184. Fax: (865) 576-5491. E-mail: agarwalpk@ornl.gov.

[1]Abbreviations: C_A, acceptor carbon; C_D, donor carbon; DHF, dihydrofolate; DHFR, dihydrofolate reductase; EcDHFR, *E. coli* dihydrofolate reductase; EVB, empirical valence bond; K32M, mutation in which lysine 32 is replaced with methionine; p-ABG, *p*-aminobenzoylglutamate; NADPH, reduced form of nicotinamide adenine dinucleotide phosphate; NADP$^+$, oxidized form of nicotinamide adenine dinucleotide phosphate; R67 DHFR, plasmid-encoded type II dihydrofolate reductase; MD, molecular dynamics.

 Published on Web 08/26/2010

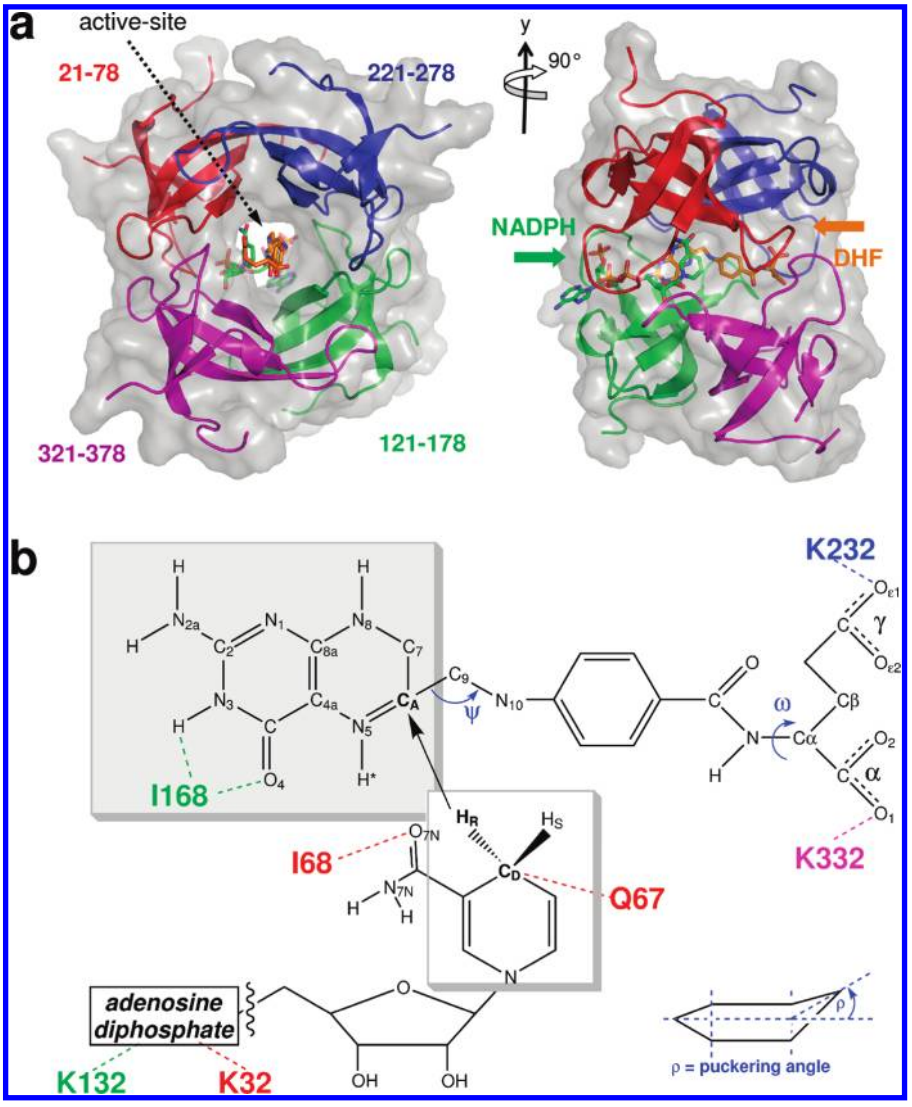

FIGURE 1: R67 DHFR structure. (a) R67 is a homotetramer possessing 222 symmetry. Each monomer is colored differently. Residues are not numbered consecutively; rather, the amino acids are labeled 1−78 for the first monomer, 101−178 for the second monomer, 201−278 for the third monomer, and 301−378 for the fourth monomer. The first 20 amino acids from each monomer were not modeled, as the first 16 amino acids are cleaved off in the fully active variant that has been crystallized (*28*) and the next four amino acids are disordered. The active site is in the middle of the pore, allowing the substrate DHF (shown as orange sticks) and cofactor NADPH (green sticks) to enter from opposite sides of the pore. (b) Important active site interactions are shown, and relevant atoms and angles are labeled (see Table S1 of the Supporting Information for a full list of important interactions). The plane of the nicotinamide ring is above that for the pteridine ring. H* denotes the protonation site.

While the R67 structure is observed to be quite rigid from NMR measurements ($\langle S_{free}^2 \rangle = 0.89$ for the apoenzyme, and $\langle S_{free}^2 \rangle = 0.86$ for R67·NADP$^+$), the *p*-aminobenzoylglutamate (p-ABG) tail of the substrate is disordered as revealed by both NMR and crystallography studies (*2*, *3*, *16*). The disorder is surprising, given the observation of a linear correlation between the ΔH associated with folate binding to the enzyme·NADPH complex (measured by isothermal titration calorimetry) and ln k_{cat}/K_m values of various mutants (*17*). Third, significant changes in enzyme active sites through mutation typically lead to decreased activity. In contrast, directed evolution experiments in R67 showed that the V66-Q67-I68-Y69 wild-type sequence can be substituted with the S66-K67-I68-H69, I66-N67-R68-Y69, or G66-E67-L68-Y69 sequence, and the mutant proteins still retain full DHFR activity (*18*). Note that as R67 is a homotetramer, changes of four residues per subunit lead to 16 mutations per active site pore!

As a model of a primitive enzyme, R67 DHFR provides an interesting opportunity to understand the factors that contribute to the catalytic efficiency of enzymes. Protein flexibility recently has been implicated in the designated function of protein scaffolds, including enzyme catalysis. EcDHFR, in particular, has been investigated with respect to the role of protein motion and flexibility in the catalytic mechanism (*19*−*21*). Conserved residues have been proposed to form a network of motions that possibly promote catalysis in the active site (*22*). The motions of the surface and other distal residues (located >10 Å from the active site) through the network are proposed to alter the chemical environment in the active site to facilitate hydride transfer (*23*). Mutation of these distal residues results in a loss of catalytic efficiency (*24*). Here, the same hydride transfer reaction is catalyzed by a completely different structural fold, albeit with differing efficiencies for EcDHFR and R67 DHFR. Therefore, a comparison of the structural interactions and motions in these two DHFRs may shed some light on how enzymes work.

In this report, we present detailed computational studies of the hydride transfer reaction catalyzed by R67 DHFR. Structural

analyses of the active site residues reveal the role of various protein regions in facilitating hydride transfer. The V66-Q67-I68-Y69 sequence from symmetry-related subunits aids in the catalytic mechanism by forming structural interactions with the substrate and cofactor. In addition, the motions of Q67 may potentially contribute to the hydride transfer reaction by helping to pucker the nicotinamide ring. Of particular interest, the p-ABG tail of DHF is quite flexible and can move between K32 residues from two different subunits during the course of the reaction. These tail movements appear to be linked to puckering of the pteridine ring, an important event during the reaction. This work provides a computational model of the hydride transfer reaction in R67 DHFR and identifies features that assist in the enzyme mechanism. Mutations of K32 in two different subunits indicate changes in catalytic activity that correlate with previous experimental observations and provide insight into the role of the p-ABG tail in the reaction mechanism. Parallels to the chromosomal DHFR catalytic reaction mechanism are also observed.

METHODS

Model Preparation. The enzyme−substrate complex was modeled using classical mechanics simulations under explicit solvent conditions. The hydride transfer reaction was modeled using the empirical valence bond (EVB) method (*25*). The AMBER (*26*) simulation package was used for model building and simulations. Note that in previous work, we have verified the suitability of AMBER's *parm98* force field for dynamics modeling with comparison with other popular force fields (*27*).

Homotetrameric R67 DHFR was modeled with one substrate and one cofactor based on the X-ray crystal structure [Protein Data Bank (PDB) entry 2RK1] (*3*). Note that the first 16 amino acids are cleaved off in the variant that has been crystallized (*28*) and the next four amino acids are disordered. Therefore, as depicted in Figure 1, all four monomers were modeled, each with 58 amino acids. The missing coordinates for the p-ABG tail of DHF were modeled using the Molecular Operating Environment (MOE Chemical Computing Group Inc.) (*29*, *30*). The model with solvent was equilibrated using a protocol described previously (*27*). All production runs were performed using AMBER version 10 (*sander* module) under NVE ensemble and periodic boundary conditions. The particle mesh Ewald method was used for electrostatic interactions; a 10 Å cutoff radius for Lennard-Jones interactions and SHAKE was used for restricting the motions of all covalent bonds with hydrogen atoms (except for the donor−hydride and acceptor−hydride bonds). For comparison, the EcDHFR enzyme complex was modeled (based on PDB entry 1RX2) using a similar protocol.

Hydride Transfer Modeled by the EVB Method. The modeled enzyme reaction is the transfer of a hydride from NADPH (cofactor) to protonated DHF to produce $NADP^+$ and THF. Hydride transfer is the rate-determining step in R67 DHFR with a rate of 1.3 s^{-1} at pH 7 (*10*). This study involves the modeling of the *pro-R* hydrogen transfer from the C4N atom on the cofactor (C_D) to the C6 atom on the protonated substrate DHF (C_A). The EVB method, in combination with classical molecular mechanics, was used for generation of the conformations along the hydride transfer reaction. The EVB method developed by Warshel and co-workers (*25*) has been used to investigate hydride transfer reactions in other enzymes (*23*, *31*). In this study, the EVB method, as implemented in AMBER version 10, was used for the simulations. The potential energy surface for the hydride transfer was described by a two-state model (shown in Figure 2)

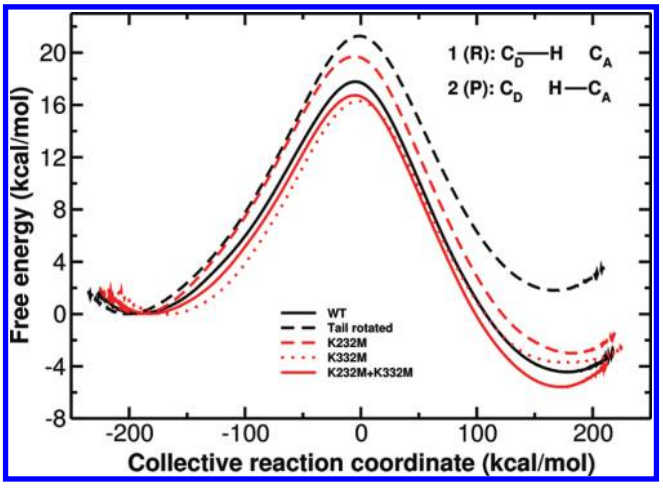

FIGURE 2: Free energy profiles for the hydride transfer reaction catalyzed by R67 DHFR. The solid black curve shows the simulations fitted to the experimental activation energy barrier (*34*), while the black dashed curve shows the profile for bound DHF where the p-ABG tail is positioned in a rotated conformation. Data from three mutants (K232M, K332M, and K232M/K332M) are colored red. The two states for the EVB calculations are shown as an inset, where 1 is the reactant state and 2 is the product state (C_D, donor carbon; C_A, acceptor carbon; and H, hydride). The transition state corresponds to the highest point of the energy profile. Two profiles for the wild-type enzyme were generated for two alternate conformations of the DHF tail; for the wild type (solid black curve), the α-carboxylate group of DHF tail interacts with K332 and the γ-carboxylate group interacts with K232, and in the tail rotated simulation (black dashed curve), the interactions are switched.

according to the Hamiltonian matrix

$$\mathbf{H} = \begin{bmatrix} V_{11} & V_{12} \\ V_{12} & V_{22} \end{bmatrix} \quad (1)$$

The bonds between the donor−hydride bond and the acceptor−hydride bond were modeled using a Morse potential:

$$V_{\mathrm{Morse}}(R_{\mathrm{CH}}) = D_e[1 - e^{\alpha(R_{\mathrm{CH}} - R_e)}]^2 \quad (2)$$

where R_{CH} is the distance between the hydride and the bonded donor or acceptor carbon atom. The parameter α, which is dependent on the force constant of the C−H bond (340 kcal/mol), is set to 1.285 A^{-1}. D_e is the dissociation constant and is 103.0 kcal/mol, while R_e is the equilibrium C−H bond length of 1.09 Å.

Because the hydride transfer reaction involves a free energy barrier greater than the thermal energy, the free energy profile was obtained with the use of a mapping potential (V_{map}):

$$V_{\mathrm{map}}(\mathbf{R};\lambda_m) = (1-\lambda_m)V_{11}(\mathbf{R}) + \lambda_m V_{22}(\mathbf{R}) \quad (3)$$

where **R** represents the positions of all atoms in the system and λ_m is the mapping parameter. The collective reaction coordinate (Λ) is defined by the equation

$$\Lambda(\mathbf{R}) = V_{22}(\mathbf{R}) - V_{11}(\mathbf{R}) \quad (4)$$

The free energy profiles were generated through a series of 19 simulations (windows) with different values of the mapping parameter λ_m ($\lambda_m = 0.05, 0.10, 0.15, ..., 0.95$).

Starting from the X-ray crystal structure, we equilibrated the solvated enzyme complex in the reactant state. For simulations with $\lambda_m = 0.05$, the coordinates were taken from the reactant state ($\lambda_m = 0$) and minimized for 5000 steps and equilibrated for 5 ps.

(Subsequently, for higher λ_m values, the starting coordinates were the equilibrated coordinates from the $\lambda_m - 0.05$ window.) The resulting coordinates (R_{eq}) served as the starting point for EVB production runs. Two independent sets of EVB production simulations were performed to test and ensure the convergence of the free energy profile. For the EVB1 set, at each λ_m, the coordinates (R_{eq}) were further minimized for 10000 steps and equilibrated for 70 ps of molecular dynamics (MD). This was followed by 700 ps production MD runs (NVE) for data collection. For the EVB2 set, at each λ_m, the coordinates (R_{eq}) were further minimized for 20000 steps and equilibrated for 70 ps of MD. This was followed by 700 ps production MD runs for data collection. Overall, this amounts to 26.6 ns of sampling for the entire reaction pathway, which was used for energy profile generation and geometrical parameter analysis. Conformations were stored every 0.1 ps, resulting in 14000 conformations (from EVB1 and EVB2 simulations) for each λ_m and 266000 conformations for the entire reaction pathway. Note that, even though the collective sampling time of 26.6 ns is much shorter than the reaction time scale of ~1 s, the use of a mapping potential (eq 3) allows sampling of the reaction pathway along the collective reaction coordinate. A similar methodology has been used for EcDHFR and other enzymes catalyzing hydride transfer (*22*, *31*).

The coupling, V_{12}, between the two valence bond states is assumed to be a constant and so is Δ_{12} (the energy adjustment term included in V_{22}), which is determined when the energy profiles are fit to the experimentally determined free energy of activation and free energy of reaction. The free energy of activation for the wild-type R67 enzyme was previously estimated to be 17.6 kcal/mol (*34*). An estimate for the free energy of reaction is currently unavailable for R67; therefore, the estimate obtained for EcDHFR of −4.4 kcal/mol was used (*23*). A V_{12} of 24.65 and a Δ_{12} of −82.95 kcal/mol lead us to values for the free energy of activation and free energy of reaction of 17.6 and −4.4 kcal/mol, respectively. The trajectory convergence was tested by comparing the two independent data sets, each of 700 ps of sampling for every λ_m. The results indicate that the EVB parameters needed to reproduce the activation energy barrier and heat of reaction differ by < 1 kcal/mol (see Figure S1 of the Supporting Information).

The mutations (K232M, K332M, and K232M/K332M) were prepared by using AMBER's *xLeap* program. Similarly, the higher-energy conformation for the wild type was prepared by rotation of the DHF tail with the *xLeap* program. The protocol described above for the wild-type enzyme was also used for these three mutants as well as an alternate p-ABG tail position in wild-type R67 DHFR to generate free energy profiles based on 26.6 ns of sampling for each system with 19 λ_m windows. The energy profiles were generated by using the wild-type EVB parameters. Note that the EVB method is expected to provide qualitative comparisons for the mutants rather than quantitatively accurate comparisons. Replicate runs were performed, and comparison of the two different sets indicates that the alternate tail and the three mutants exhibit similar trends for the activation energy barrier (higher or lower barrier than that of the wild-type enzyme); however, quantitatively, the barriers show variations of 1−2 kcal/mol between the two data sets (see Table S2 of the Supporting Information). The validation of the energy surface for hydride transfer could be provided by comparison of the EVB-optimized transition state structure with ones obtained from quantum mechanical models. The EVB-optimized transition state structure could be obtained in a way similar to electronic structure calculations (where the saddle point is located by optimizing the structure until the diagonalized Hessian shows only one negative eigenvalue). At present, software for computing such an EVB-optimized structure is not available. Therefore, an averaged structure based on the reaction trajectories crossing the EVB diving surface (highest point on the free energy profile) and a density functional theory-optimized structure for an active-site model are provided as Supporting Information.

A similar protocol was used for EcDHFR, but only 100 ps of sampling was performed for each λ_m window. Note that EcDHFR simulations were performed for comparison of the DHF tail angle. Even with a relatively small sampling, the DHF tail angle result shows exactly the same behavior that was previously described (*23*).

Equilibrium Geometrical Properties. Variations of the geometrical quantities (interactions, distances, and angles) over the course of the hydride transfer were computed as a function of the reaction coordinate. These quantities were extracted from each of the 266000 conformations sampled along the reaction pathway (collected from the separate sets of trajectories as described above) and were sorted into histograms (bin size of 1 kcal/mol) based on the value of the reaction coordinate associated with the conformation (eq 4). The average value of the geometrical parameter value per bin was used in analysis (a running average of 20 bins was used for the final plots). The state of hybridization for the donor and acceptor was calculated on the basis of the methodology described by Truhlar, Gao, and co-workers (*32*). In addition to the equilibrium properties, the 266000 conformations were also used for quasi-harmonic analysis to investigate enzyme flexibility (see the Supporting Information for details).

Radius of Gyration. The radius of gyration (R_g) for substrate DHF was computed according to the following equation:

$$R_g = \left\{ \frac{1}{M} \left\langle \sum_{k=1}^{N} m_k [(x_k - x_{COM})^2 + (y_k - y_{COM})^2 + (z_k - z_{COM})^2] \right\rangle \right\}^{1/2} \quad (5)$$

where M is the total molecular mass, N is the number atoms in the molecule, m is the mass of an atom, x, y, and z indicate the Cartesian coordinates of an atom, and x_{COM}, y_{COM}, and z_{COM} indicate the coordinates of the center of mass of the molecule. Note that R_g provides mass-weighted root-mean-square displacements for the substrate molecule and is mostly affected by p-ABG tail movement as the pteridine ring remains rigidly docked at the center of the pore.

RESULTS

The free energy profile for the hydride transfer reaction catalyzed by R67 DHFR was obtained using the EVB method. Figure 2 shows the reactant and product states for the reaction used for two-state implementation of the EVB method and the resulting energy profiles. On the basis of previous models (*23*, *33*), our model invokes one possibility in which N5 protonation occurs before the hydride transfer. Because the p-ABG tail of DHF is disordered in the X-ray crystal structure, two initial conformations were built with the α- and γ-carboxylates switched with respect to their interactions with symmetry-related K32 residues. These profiles as well as those for three K32M mutant enzymes (discussed below) are shown in Figure 2. The EVB parameters, V_{12} and Δ_{12}, were selected to reproduce the experimental barrier height

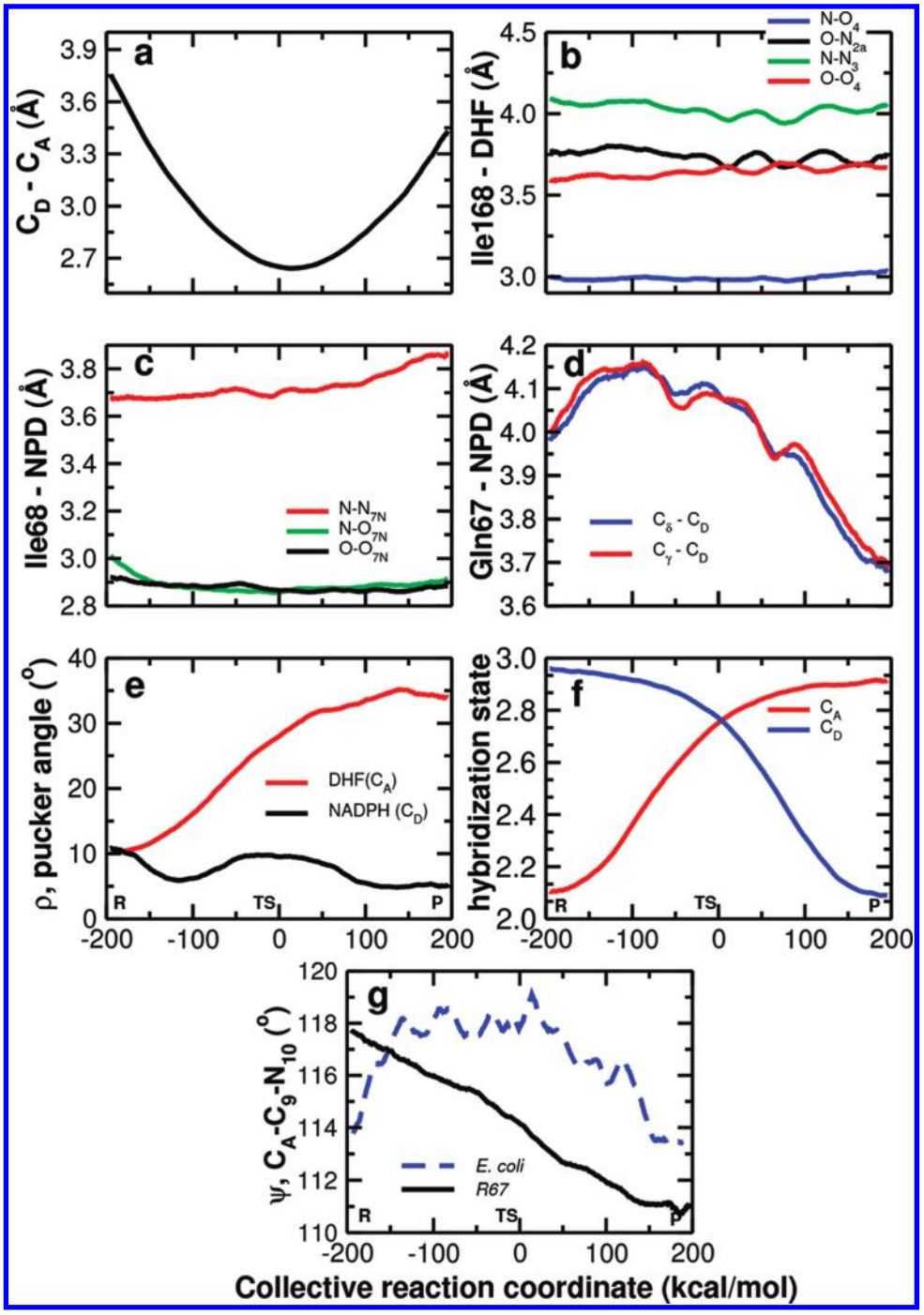

FIGURE 3: Equilibrium averages of geometrical properties along the collective reaction coordinate. (a) Donor and acceptor carbon distance. (b) Various interactions between I168 and the N2a, N3, and O4 atoms of DHF. (c) Distances between I68 and the carboxamide group in the nicotinamide ring of the cofactor. (d) Interaction distance between Q67 and the donor carbon. (e) Ring puckering angle as defined in Figure 1b. (f) State of hybridization for donor and acceptor carbons. (g) DHF tail angle (indicated as ψ in Figure 1b). The reactant (R, reaction coordinate of −191.5 kcal/mol) and product (P, reaction coordinate of 178.0 kcal/mol) are defined as the lowest points in the free energy profile of Figure 2 (for comparison, the EcDHFR reactant and product states are located at −160 and 180 kcal/mol, respectively).

for the wild-type R67 enzyme ($\Delta G^{\ddagger} = 17.6$ kcal/mol) (*34*), while the free energy of the reaction was fixed to the experimental value for EcDHFR (−4.4 kcal/mol) (*23*). The parameters, V_{12} and Δ_{12}, obtained by fitting the wild-type enzyme, were used for the simulations with the alternate tail conformation and the three mutants to allow a comparison of the energy landscapes. Previously, such a comparison has been used by Warshel and coworkers to investigate hydride transfer in EcDHFR (*35*).

As identified in the ternary complex crystal structure (*3*), many enzyme−substrate interactions in the active site allow the pteridine ring of the substrate to be held close to the nicotinamide ring of the cofactor (see Figure 3). As depicted in Figure 3a, the enzyme active site enables the donor carbon−acceptor carbon (C_D−C_A) distance to decrease to 2.6−2.8 Å at the transition state. This behavior has previously been reported for other enzyme-catalyzed hydride transfer reactions (*36*) and is similar to the decrease seen in EcDHFR (*22*). It has been suggested that a decrease in the C_D−C_A distance is required for a larger overlap of the hydride (nuclear) wave function associated with the reactant and product states (*23*). An *endo* configuration between the

reactive rings proposed for both the ground state (*3*, *16*) and the transition state (*37*, *38*) requires the C_D-H-C_A angle to be >100° for hydride transfer to occur. In our simulations, this angle increases from ~130° in the reactant state to 165.8° in the transition state (see Figure S2 of the Supporting Information), with a subsequent decrease to ~145° in the product state. The computed EVB transition state geometry is based on the average of ~1300 enzyme conformations that are located in the vicinity of the maximum in the free energy profile (corresponding to the reactive trajectories that cross the dividing surface in the EVB framework). To check this transition state geometry, we additionally used electronic structure calculations at the DFT/B3LYP/6-31G** level (see Figure S3 of the Supporting Information). The obtained transition state geometries from the two methods are similar.

Active Site Interactions with DHF and NADPH. Important interactions between R67 and its substrate and cofactor were identified using dynamical cross-correlation coefficients calculated over the course of the entire hydride transfer pathway (see Figure S4 of the Supporting Information). The largest correlations with bound DHF as well as cofactor NADPH are shown by K32 and the V66-Q67-I68-Y69 regions from the four subunits. To improve our understanding of the role of these regions in enzyme function, these various interactions were monitored as a function of distance and angle over the course of the hydride transfer reaction. As depicted in Figure 3b, there are one strong and three weak (*39*) hydrogen bonds formed between the backbone atoms of I168 and the DHF pteridine ring that allow the substrate to be held close to the cofactor. These H-bonding interactions are maintained during the entire reaction profile, preventing any large movements of the pteridine DHF ring. Additionally, the alkyl side chain of I168 provides hydrophobic interactions with the pteridine ring. As an interesting coincidence, the backbone atoms of I68 (same residue from another subunit) form strong H-bonds with the nicotinamide carboxamide in the cofactor NADPH (see Figure 3c), also allowing this portion of the cofactor to be held rigidly. Additional interactions along the length of the NADPH molecule constrain its position during the reaction profile. In particular, K32 and K132 form ion pairs with the phosphate groups.

Glutamine 67 forms close interactions with the nicotinamide ring of NADPH, particularly with the hydride donor carbon (C_D). The side chain of Q67 shows relatively stable hydrophobic interactions with C_D (see Figure 3d) for the first half of the reaction when the Q67 $C_\delta-C_D$ and Q67 $C_\gamma-C_D$ distances are ~4.1−4.2 Å; however, as the reaction proceeds from the transition state to the product state, these distances quickly decrease to 3.7 Å, possibly indicating a change in the chemical environment at C_D. These Q67 C_D distance changes occur simultaneously with the puckering of the nicotinamide ring (see Figure 3e). Collectively, these changes show a change in the hybridization state of C_D going from sp^3 to sp^2, aiding in the loss of the hydride (see Figure 3f). This behavior has also been observed in EcDHFR (*32*).

Puckering of the nicotinamide ring has been thought to contribute to the reaction coordinate in the dinucleotide (NADPH/NADH) binding enzymes (*40*, *41*). Note that variation in the NADPH cofactor ring puckering in R67 (as depicted in Figure 3e) is consistent with previous results based on detailed quantum level modeling. In those studies, localized molecular orbital analysis indicated that small changes (5−10°) in cofactor ring puckering are sufficient to alter the electronic environment at the C_D (*42*, *43*).

The chemical environment of the acceptor carbon (C_A) also shows changes suitable for the incoming hydride. The most important change is puckering of the pteridine ring (see Figure 3e), occurring simultaneously with changes in the DHF tail angle, going from 118° (corresponding to sp^2-like character of C_A) to 111° (sp^3-like character for C_A) as depicted in Figure 3g. However, despite a close inspection of enzyme−substrate interactions, it remains unclear what residues are associated with this change. This is particularly intriguing because the shortest interactions with C_A are made by the side chain of Q167, which is >4.2 Å away. In EcDHFR, it was suggested that movement of the DHF tail, along with positioning of F31, aids in controlling the environment at C_A (*22*). However, in R67, both NMR and X-ray crystallography experiments indicate the p-ABG tail of DHF is disordered (*2*, *3*, *16*). Therefore, the reaction-coupled flexibility of R67 during the course of hydride transfer was characterized to understand the behavior of the DHF tail as well as the possible impact of motions of various residues on the reaction mechanism. The results indicate that atoms and residues at the center of the pore are mostly rigid while the regions around the edge of the pore, including those involving the K232 and K332 residues, show the largest degree of flexibility (see Figure S5 of the Supporting Information).

Analysis of the Role of the DHF Tail. The impact of p-ABG tail flexibility was characterized with respect to its ability to induce changes in the DHF tail angle. Analysis of computational simulations shows that the p-ABG tail, surrounded mostly by solvent, can freely move in the pore with its α- and γ-carboxylate groups forming ion pairs and/or solvent-separated ion pairs with residues K232 and K332. These observations are consistent with the disorder seen in NMR and crystallography studies (*2*, *3*, *16*). For the wild-type enzyme, K232 forms an ion pair with the γ-carboxylate group of the p-ABG tail while the symmetry-related K332 residue shows a longer and often solvent-separated ion pair with the α-carboxylate group (see Figure S6 of the Supporting Information). Over the course of the reaction, the ion pair between K232 and the γ-carboxylate group fluctuates between 3 and 4 Å, while the solvent-separated interaction between K332 and the α-carboxylate group fluctuates between 4.5 and 5.5 Å as the tail moves around in the middle of the pore (see Figure S7 of the Supporting Information). The flexibility of the DHF tail also raises an important concern regarding the interaction of the K232 and K332 residues with the γ- and α-carboxylate groups in an alternate conformation, where the interactions are reversed. Here, K232 forms an ion pair with the α-carboxylate group, while K332 interacts with the γ-carboxylate group of DHF. As depicted in Figure 2, this conformation shows a higher barrier for hydride transfer.

Simulations indicate that the DHF tail is able to rotate freely between two alternate conformations (see Figure 4). A 5 ns MD trajectory in the ground (reactant) state indicates that the tail rapidly rotates back and forth between the two conformations as indicated by a change in the dihedral angle associated with the carboxylate groups (labeled ω in Figure 1b). This trajectory is depicted in Figure 4a. The dihedral angle switching between the two states (A and B) indicates the tail's ability to rotate freely between two alternate conformations. In this ground state trajectory for the wild-type enzyme, the tail position starts in state A, where the α-carboxylate group interacts with K232 and the γ-carboxylate group interacts with K332. In this state, ω ranges between 240° and 300°. After ~1.3 ns, the tail rotates to state B, where ω ranges between 150° and 210° and the

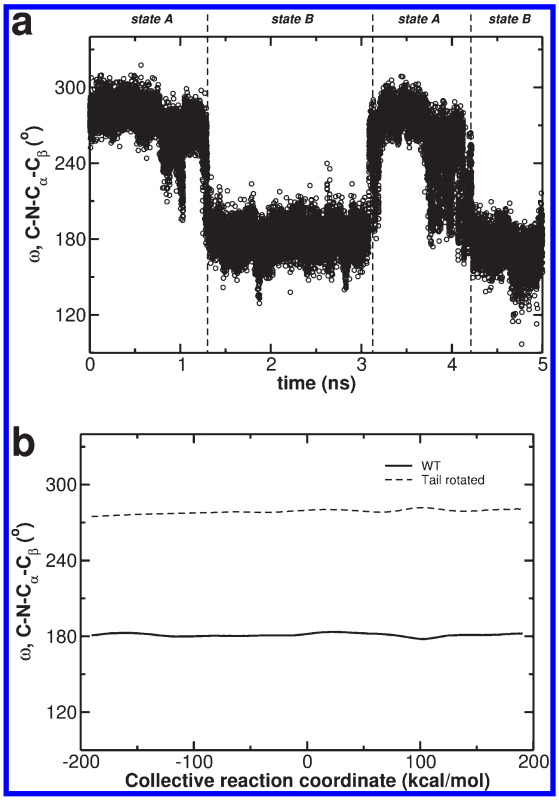

FIGURE 4: Glutamate tail dynamics. (a) Rotation of the glutamate tail in DHF monitored in a 5 ns ground state MD simulation. State A corresponds to bound DHF with its α-carboxylate interacting with K232 and γ-carboxylate group interacting with K332, while state B corresponds to bound DHF with its γ-carboxylate interacting with K232 and α-carboxylate group interacting with K332. (b) Tail angle over the course of the reaction pathway for the wild-type enzyme reaction (corresponding to state B) and the alternate conformation (corresponding to state A and higher energy barrier in Figure 2). Note that the ground state trajectory depicted in panel a was started in the tail conformation corresponding to the higher energy barrier in Figure 2.

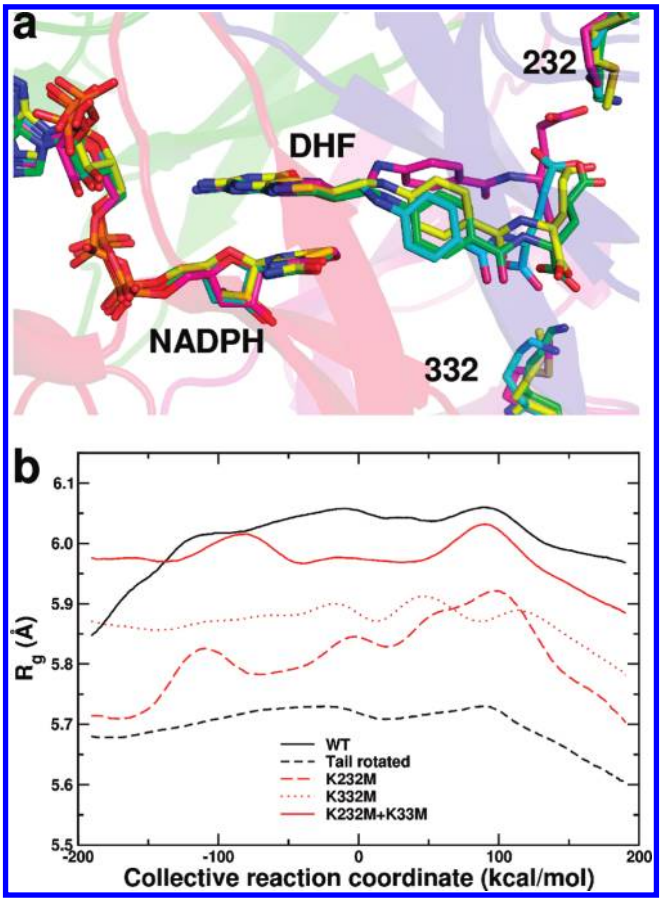

FIGURE 5: Impact of K232 and K332 mutations on DHF tail flexibility. (a) Average substrate and cofactor orientation at the transition state for the wild type (substrate, cofactor, and residues K232 and K332 shown as green sticks), the single K232M mutant (cyan sticks), the single K332M mutant (magenta sticks), and the double K232M/K332M mutant (yellow sticks). The average structures are based on ~1000 conformations present within ±3 kcal/mol of the reaction coordinate from the transition state (defined as the highest point of the energy profile in Figure 2). (b) Radii of gyration (R_g) of DHF when bound to either the wild-type enzyme or the mutants. Note that R_g is mostly affected by p-ABG tail movement as the pteridine ring remains rigidly docked at the center of the pore.

interactions of the carboxylate groups with K232 and K332 are switched. As the simulation continues, switching back and forth readily occurs between these two states. Collectively, these results indicate that even though the pteridine ring is held fixed in the rigid environment of the active site, the DHF tail constantly samples a range of conformations in the solvent accessible area of the pore. This sampling is enabled by the inherent tail flexibility and the population of species incurred upon switching of the ion pairs between the α- and γ-carboxylate groups of the DHF tail with symmetry-related K232 and K332 residues present at the edge of the pore. The disordered tail in the X-ray and NMR structures presumably is a result of this flexibility. Note that the trajectories used for the EVB free energy profiles for the wild type (state B) and the alternate DHF tail conformation (tail rotated) show no switching between the two states, possibly due to only a 0.7 ns simulation in each λ_m window. As depicted in Figure 4b, in the energy profile with the lower energy barrier (solid black curve in Figure 2), the DHF tail samples only state B, while the energy profile with the rotated tail (black dashed curve in Figure 2) shows a higher energy barrier and samples only state A.

Mutation of K232 and K332 to methionine provides additional insight into the possible role of these residues in the reaction (see Figures 2 and 5). A single K232M mutation indicates that the loss of the ion pair between the γ-carboxylate group and K232 leads to an increase in the activation energy barrier, while the loss of interactions between K332 and the α-carboxylate group leads to a decrease in the barrier. Interestingly, the double mutation (K232M/K332M) also indicates better catalysis due to a lowered barrier. A comparison of the structures at the transition state for the wild type and three mutants provides vital clues about the role of DHF tail flexibility during the course of the reaction. The average structures at the transition state (see Figure 5a) reveal that the tail in the wild type and double mutant has more or less the same conformation, while for the K232M mutant, the tail interacts more strongly with K332 because of the loss of the interactions with M232. Similarly for the K332M mutant, the average tail position is pulled toward K232 because of the loss of the interactions with M332. [A comparison of averaged structures in the reactant and product states also indicates similar results (see Figure S8 of the Supporting Information).] In the single mutants, the loss of one ion pair leads to a shift in the average tail position, eventually impacting the environment at C_A because of a shift in the DHF tail angle. This is supported by the computational prediction that the average tail position for the double mutant with the loss of interactions at both K32 positions is almost the same as in the wild type, where both interactions are present. As depicted in

Figure S9 of the Supporting Information, the tail is able to rotate very rapidly (with the DHF tail angle, ψ, varying between 105° and 125°) on the picosecond time scale; however, the averaged value of the tail angle depends on the identity of the amino acids at positions 232 and 332. Because the lifetimes of these states are extremely short (~0.1 ns), it is possible that a reaction trajectory (corresponding to a k_{cat} of ~1 s^{-1}) is only successful if it coincides with the correct changes in the other enzyme−substrate interactions, including the environment at C_D. Further, the loss of DHF tail interactions with K232 and K332 appears to favor an increased rate of the enzyme, as indicated by a lower energy barrier for the single K332M mutant and the double mutant, where the loss of ion pair interactions with the carboxylate groups allows more conformational sampling. The single K232M mutant appears to be different, as the loss of an ion pair at this position leads to a distortion of the dihedral angle at the C_A (i.e., N5−C_A−C9−N10). As shown in Figure S10 of the Supporting Information, this dihedral angle is different in the K232M mutant and the wild type and the other two mutants and, therefore, could indicate an unfavorable consequence for the hydride transfer event. Note that even though the tail conformation in the K332M mutant appears to have an orientation different from the other three cases due to the strong ion pair with K232, a dihedral angle (N5−C_A−C9−N10) distortion is not observed, and in fact, this orientation appears to favor the change in the DHF tail angle (see Figures S8 and S9 of the Supporting Information and discussion below).

A comparison of the radii of gyration (R_g) for the substrate DHF, over the course of hydride transfer, provides supporting evidence for the linkage between DHF tail flexibility and the height of the energy barrier (see Figure 5b). The wild-type enzyme with bound DHF in state B shows the largest value of R_g, whereas the smallest R_g values are associated with the wild-type enzyme with bound DHF in state A (rotated tail) as well as the K232M mutant. These different R_g values correlate with low and high energy barriers in Figure 2. The double mutant also shows a large R_g across the entire reaction profile, possibly because of a lack of interactions between the DHF carboxylate groups and the enzyme. This may enable the DHF tail angle to be sampled at a slightly faster rate, perhaps providing an explanation for the lower energy barrier. As well as trends in R_g correlating with the energy barrier height, there may be several other contributing factors, such as various angles associated with the tail orientation. It is difficult to quantitatively estimate the impact of these contributing factors on changes in barrier heights as a large range of possible motions are available to the p-ABG tail in both wild-type and mutant configurations. Nonetheless, Table S3 of the Supporting Information summarizes a qualitative comparison of the DHF tail angle and the N5−C_A−C9−N10 dihedral angle as potential factors contributing to a change in barrier height compared to that of the wild-type enzyme. This analysis suggests that in addition to the R_g value, sampling of the DHF tail angle, ψ, in the 114−116° range may be important for achieving the transition state (see Figure S11 of the Supporting Information). For example, the K332M mutant, even though its R_g value is only intermediate, does show a slight lowering of the energy barrier. As mentioned above, for the K332M mutant, the DHF tail is oriented differently (see Figure 5a). For this mutant, the DHF tail angle, ψ, shows a value of ~116° in the ground and reactant states of the reaction pathway (see Figure S11 of the Supporting Information). Therefore, for the K332M mutant, it appears that the combination of an intermediate R_g value and a decreased value for the DHF tail angle possibly provides an overall beneficial change to the electronic environment at the C_A. Interestingly, the wild-type enzyme with bound DHF in state A (rotated tail) also shows a decreased value of ψ between the reactant and transition states (see Figure S11 of the Supporting Information) because of its altered conformation. However, it has the smallest R_g value indicating the lowest flexibility. Therefore, as summarized in Table S3 of the Supporting Information, it appears that for wild-type enzyme with the bound substrate possessing an alternate tail conformation(s) (even though the tail angle is favorable), a significantly lower flexibility (smallest R_g) may provide an explanation for a slower hydride transfer rate. Collectively, analysis of the DHF tail in the wild type and mutants suggests that a favorable combination of the tail orientation and flexibility may be required to induce the required change in the DHF tail angle, which in turn likely controls the state of hybridization of the C_A.

DISCUSSION AND SUMMARY

The computational results presented here provide insight into the mechanism of R67 DHFR catalysis. In the active site, the proximity of NADPH and DHF is achieved by numerous strong interactions with enzyme residues. During catalysis, bound NADPH remains reasonably rigid as does the pteridine ring of DHF. Water is excluded by constriction of the central portion of the pore. Stacking of the nicotinamide and pteridine rings [as also seen in the NMR and X-ray structures (*3*, *16*)] enables use of the more stable *endo* transition state (*37*, *38*). The observations made here are consistent with previous suggestions of NADPH ring puckering being a significant contributor to the reaction coordinate (*41*, *44*). As shown in Figure 3d, activation of NADPH may be achieved in R67 DHFR by motion of Q67, which is positioned behind the C_D position of the nicotinamide ring, resulting in ring puckering and ultimately hydride transfer. A different mechanism appears to be operative in DHF, as pteridine ring puckering appears to be achieved by rigid binding of the pteridine ring coupled to movement of the p-ABG tail between symmetry-related K232 and K332 residues.

The flexibility of the substrate's p-ABG tail at the edge of the active site is paradoxical as it contrasts with the paradigm that enzymes hold their substrates in fixed positions (*12*−*15*). The disordered tail implies the ability to sample the large volume at the end of the pore. Previous docking studies have predicted that the tail can sample various conformations between the two extreme states, where the carboxylate groups form ion pairs with K32 residues from two different subunits (*4*, *45*). The computational studies presented here indicate tail movement can alter the chemical environment on the acceptor carbon by inducing a change in the state of hybridization. Previous resonance Raman studies provide supporting evidence of this computational prediction as two C6=N5 bond stretches are observed for DHF when bound to an H62C mutant R67 DHFR·$NADP^+$ complex (*46*). Deng et al. note the orientation of the R group off the C6 position significantly impacts the C6=N5 stretch, suggesting the observed split of the C6=N5 signal correlates with two binding modes for DHF where the p-ABG tail adopts different orientations.

Our computational results predict that movement of the p-ABG tail between symmetry-related K32 residues leads to alterations in the structure of DHF, in particular puckering of the pteridine ring. As ring puckering lies on the path to transition

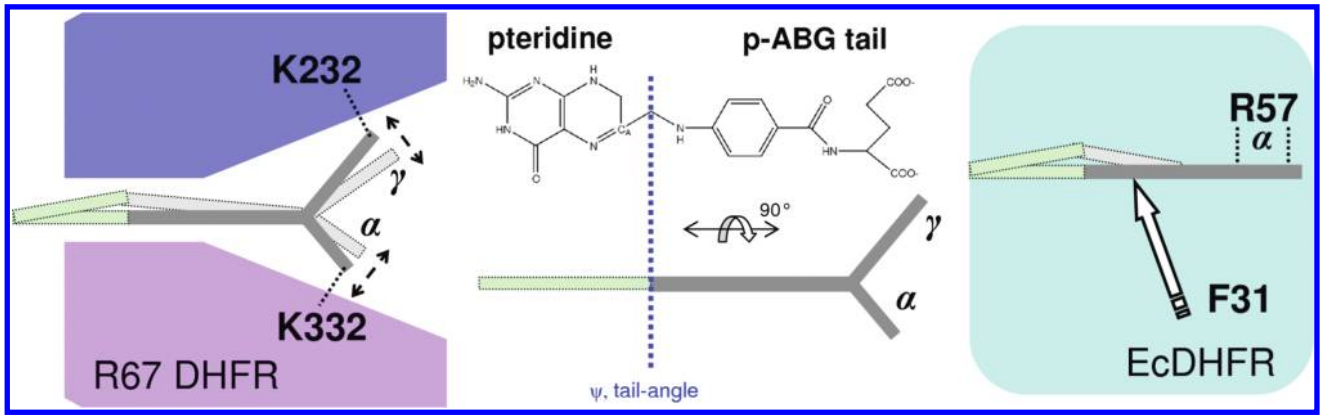

FIGURE 6: Comparison of DHF tail flexibility in R67 DHFR and EcDHFR. In R67, the large flexibility of the tail arises because of its ability to sample the large space at the end of the pore. This occurs due to alternative interactions between the α- and γ-carboxylate groups and the K332 and K232 residues, which appear to enable a change in the DHF tail angle suitable for hydride transfer. As the protein scaffold allows a large degree of movement at the edge of the active site pore, this results in a continuous change in ψ in Figure 3g. In EcDHFR, the α-carboxylate group is rigidly held by R57 while F31 motions are proposed to induce changes in the DHF tail angle. As DHF is bound in a cleft and the Met20 loop closes over bound ligands in EcDHFR, this structure constrains the ability of the p-ABG tail to move; thus, ψ in Figure 3g shows a different pattern than in R67 DHFR. Note that the colored areas indicate a cross section of the relevant areas of the enzyme. In R67 DHFR, the cross section shows the full width of the pore, while in EcDHFR, it indicates interaction of DHF with specific enzyme residues.

state formation, disorder of the DHF tail may serve a functional role. [While it is difficult to distinguish cause and effect here, we note flexibility is present in the ground state and nonreactive states (such as the two folate or DHF·NADP$^+$ crystal structures), indicating that flexibility is not solely driven by catalysis.] This hypothesis is supported by numerous experimental observations. First is the observation of a large contribution of entropy to R67 catalysis ($T\Delta S^{\ddagger}_{25} = -11.3$ kcal/mol) (*34*). A second experimental result that supports our hypothesis is the observation that addition of salt (ionic strength of up to 0.42) enhances k_{cat} 2.5-fold (*47*). This observation is unusual as salt effects typically alter ligand binding rather than k_{cat}. The slope of a log−log plot of k_{cat} versus ionic strength (NaCl) in wild-type R67 DHFR is approximately 1, consistent with the breakage of a salt bridge going from the ground state to the transition state. This study predicts the salt sensitive interaction is a salt bridge between the α-/γ-carboxylate moiety in the p-ABG tail of DHF and K32. Additionally, kinetic isotope effect experiments, conducted at increasing ionic strengths as well as theoretical calculations, suggest electrostatic repulsion between the H donor and H acceptor is weakened, and the reaction coordinate is better organized for H tunneling (*48*). Finally, a single K32M mutant as well as all double K32M mutants were constructed in a tandem array of four fused R67 DHFR genes (*49*). This approach allowed asymmetric addition of mutations in a monomeric protein possessing the essential tertiary structure of R67 DHFR. For the double mutants with K32M mutations appearing on both sides of the pore, the k_{cat} decreased 4−8-fold. For the double mutant with K32M mutations on one side of the pore (K232M/K332M), k_{cat} increased 4-fold, consistent with a decreased activation energy barrier that was observed in the computational results (Figure 2). From previous binding studies, NADPH has been proposed to bind before DHF (*7*), and from crystal structure analysis (*3*), NADPH interacts tightly with R67 using ion pairs with K32 residues. Thus, initial binding of NADPH to the unmutated half of the pore in the K232M/K332M asymmetric mutant is proposed to be followed by binding of DHF to the mutant (K32-less) half of the pore. From this binding model, loss of the ion pairing capability in the DHF binding site appears to correlate with an increase in k_{cat}, again agreeing with the computational predictions in Figure 2. Finally, the interactions of K32 with DHF were found to be important in binding (as seen in the K232M/K332M mutant); however, they could be eliminated if compensatory Q67H mutations (which tighten binding) were added (*50*). A further discussion of the asymmetric K32 mutants is given in the Supporting Information.

Overall, these results indicate that ion pairing between the K32 residues and the DHF carboxylates is important in ground state binding of substrate. However, because of the symmetry of R67 DHFR and the promiscuous binding surface, loss of this interaction(s) is needed for the enzyme to reach the transition state. Thus, mutations that increase DHF tail flexibility in the pore and remove the ground state ion pair interactions appear to lead to increased catalytic efficiency.

Comparison of EcDHFR and R67 DHFR Catalytic Strategies. Despite the structural differences between R67 DHFR and EcDHFR, both enzymes catalyze the same chemical reaction. While R67 DHFR uses an *endo* transition state and EcDHFR uses an *exo* transition state, the computational results presented here suggest some similarities with respect to how these two enzymes provide crucial structural interactions in the active site. Further, there are similarities with regard to the relative motions, both in the center and on the edge of the active site, that alter the chemical environment making it suitable for catalysis to occur. In particular, puckering of the NADPH ring and a change in the DHF tail angle are observed in both enzyme systems. In EcDHFR, the nicotinamide ring puckering motion has been suggested to be induced by a network of coupled motion originating from D122 on the surface and terminating in Y100 in the active site, positioned behind the C_D (*22*). In R67 DHFR, the Q67 side chain appears to provide similar motions to the C_D atom, also positioned behind the cofactor ring. The most interesting difference in the enzyme mechanism appears to impact the chemical environment at the C_A (see Figure 6). While changes in the DHF tail angle are observed (that lead to a change in the C_A hybridization state from sp^2 to sp^3) for both R67 DHFR and EcDHFR, the pattern along the reaction coordinate differs (see Figure 3g). This likely arises because of differences in active site volume, which either constrains tail movement (EcDHFR) or

allows large movements at the edge of the pore (R67). In EcDHFR, it has been suggested that motions of the F31 side chain provide promoting motions that alter the DHF tail angle, thereby making the C_A atom more suitable for the incoming hydride. In R67 DHFR, our computational studies predict that the same change in the chemical environment results from the p-ABG tail movement. Sampling of the DHF tail angle is made possible by the large flexibility of the tail located at the edge of the pore surrounded by bulk solvent. The two extreme states for the conformations are ion pairs between the α- and γ-carboxylate groups of DHF interacting with symmetry-related lysines from two different subunits (K232 and K332).

To conclude, we consider negative design (i.e., blocking of undesired alternatives), which has been proposed as a necessary consideration in protein design efforts (*51*−*53*) and likely occurs in enzyme evolution as well. Evolutionary steps toward a smoother binding funnel and lower transition state surface have probably been hidden in well-evolved enzymes; thus, examination of the R67 DHFR mechanism can help uncover these design elements. For example, one feature consistent with R67 being a primitive enzyme is imposition of 222 symmetry on its single active site, which does not allow optimization of cofactor and DHF binding. While K32 is important in ground state binding of DHF, it appears that loss of this interaction is necessary to reach the transition state as shown by experiment (*47*) and predicted by this computational study as well. Another issue in R67 catalysis is p-ABG tail movement. While the flexibility of the p-ABG tail in R67 DHFR appears to correlate with pteridine ring puckering and ultimately catalysis, this movement samples a large conformational space that allows variable DHF tail angles. These values vary depending on how the p-ABG tail is bound or which K32 mutants are considered. If specific conformational fluctuations result in better coupling with catalysis, perhaps EcDHFR uses negative design to achieve DHF ring puckering by the more subtle movement of F31 against the back side of the pteridine ring.

ACKNOWLEDGMENT

We thank Hong Guo and Robert Beahm for their initial modeling studies on R67 DHFR and Kim Wong for help with EVB scripts.

SUPPORTING INFORMATION AVAILABLE

A movie depicting enzyme flexibility along the reaction pathway; comparison of the free energy profiles from the two EVB sets used in this study; barrier heights for mutant systems; transition state geometry; cross-correlation plots for enzyme and the substrate and cofactor; reactant-coupled enzyme flexibility; variation of interactions between K232 and K332 and the DHF tail; DHF tail angles; and N5−C_A−C9−C10 dihedral angle variation along the reaction coordinate for wild-type and mutant enzymes. This material is available free of charge via the Internet at http://pubs.acs.org.

REFERENCES

1. Howell, E. E. (2005) Searching sequence space: Two different approaches to dihydrofolate reductase catalysis. *ChemBioChem 6*, 591–600.
2. Narayana, N., Matthews, D. A., Howell, E. E., and Xuong, N. H. (1995) A Plasmid-Encoded Dihydrofolate-Reductase from Trimethoprim-Resistant Bacteria Has a Novel D-2-Symmetrical Active-Site. *Nat. Struct. Mol. Biol. 2*, 1018–1025.
3. Krahn, J. M., Jackson, M. R., DeRose, E. F., Howell, E. E., and London, R. E. (2007) Crystal structure of a type II dihydrofolate reductase catalytic ternary complex. *Biochemistry 46*, 14878–14888.
4. Alonso, H., Gillies, M. B., Cummins, P. L., Bliznyuk, A. A., and Gready, J. E. (2005) Multiple ligand-binding modes in bacterial R67 dihydrofolate reductase. *J. Comput.-Aided Mol. Des. 19*, 165–187.
5. Brisson, N., and Hohn, T. (1984) Nucleotide sequence of the dihydrofolate-reductase gene borne by the plasmid R67 and conferring methotrexate resistance. *Gene 28*, 271–274.
6. Sawaya, M. R., and Kraut, J. (1997) Loop and subdomain movements in the mechanism of *Escherichia coli* dihydrofolate reductase: Crystallographic evidence. *Biochemistry 36*, 586–603.
7. Bradrick, T. D., Beechem, J. M., and Howell, E. E. (1996) Unusual binding stoichiometries and cooperativity are observed during binary and ternary complex formation in the single active pore of R67 dihydrofolate reductase, a D-2 symmetric protein. *Biochemistry 35*, 11414–11424.
8. Smith, S. L., and Burchall, J. J. (1983) α-Pyridine Nucleotides as Substrates for a Plasmid-Specified Dihydrofolate Reductase. *Proc. Natl. Acad. Sci. U.S.A. 80*, 4619–4623.
9. Jackson, M., Chopra, S., Smiley, R. D., Maynord, P. O., Rosowsky, A., London, R. E., Levy, L., Kalman, T. I., and Howell, E. E. (2005) Calorimetric studies of ligand binding in R67 dihydrofolate reductase. *Biochemistry 44*, 12420–12433.
10. Yahashiri, A., Howell, E. E., and Kohen, A. (2008) Tuning of the H-transfer coordinate in primitive versus well-evolved enzymes. *ChemPhysChem 9*, 980–982.
11. Calderone, C. T., and Williams, D. H. (2001) An enthalpic component in cooperativity: The relationship between enthalpy, entropy, and noncovalent structure in weak associations. *J. Am. Chem. Soc. 123*, 6262–6267.
12. Williams, D. H., Stephens, E., and Zhou, M. (2003) How can enzymes be so efficient? *Chem. Commun.,* 1973–1976.
13. Williams, D. H., Stephens, E., and Zhou, M. (2003) Ligand binding energy and catalytic efficiency from improved packing within receptors and enzymes. *J. Mol. Biol. 329*, 389–399.
14. Snider, M. J., Gaunitz, S., Ridgway, C., Short, S. A., and Wolfenden, R. (2000) Temperature effects on the catalytic efficiency, rate enhancement, and transition state affinity of cytidine deaminase, and the thermodynamic consequences for catalysis of removing a substrate "anchor". *Biochemistry 39*, 9746–9753.
15. Wolfenden, R. (2003) Thermodynamic and extrathermodynamic requirements of enzyme catalysis. *Biophys. Chem. 105*, 559–572.
16. Li, D. W., Levy, L. A., Gabel, S. A., Lebetkin, M. S., DeRose, E. F., Wall, M. J., Howell, E. E., and London, R. E. (2001) Interligand overhauser effects in type II dihydrofolate reductase. *Biochemistry 40*, 4242–4252.
17. Strader, M. B., Chopra, S., Jackson, M., Smiley, R. D., Stinnett, L., Wu, J., and Howell, E. E. (2004) Defining the binding site of homotetrameric R67 dihydrofolate reductase and correlating binding enthalpy with catalysis. *Biochemistry 43*, 7403–7412.
18. Schmitzer, A. R., Lepine, F., and Pelletier, J. N. (2004) Combinatorial exploration of the catalytic site of a drug-resistant dihydrofolate reductase: Creating alternative functional configurations. *Protein Eng., Des. Sel. 17*, 809–819.
19. Benkovic, S. J., and Hammes-Schiffer, S. (2003) A perspective on enzyme catalysis. *Science 301*, 1196–1202.
20. Garcia-Viloca, M., Truhlar, D. G., and Gao, J. L. (2003) Reaction-path energetics and kinetics of the hydride transfer reaction catalyzed by dihydrofolate reductase. *Biochemistry 42*, 13558–13575.
21. Thorpe, I. F., and Brooks, C. L. (2005) Conformational substates modulate hydride transfer in dihydrofolate reductase. *J. Am. Chem. Soc. 127*, 12997–13006.
22. Agarwal, P. K., Billeter, S. R., Rajagopalan, P. T. R., Benkovic, S. J., and Hammes-Schiffer, S. (2002) Network of coupled promoting motions in enzyme catalysis. *Proc. Natl. Acad. Sci. U.S.A. 99*, 2794–2799.
23. Agarwal, P. K., Billeter, S. R., and Hammes-Schiffer, S. (2002) Nuclear quantum effects and enzyme dynamics in dihydrofolate reductase catalysis. *J. Phys. Chem. B 106*, 3283–3293.
24. Wang, L., Goodey, N. M., Benkovic, S. J., and Kohen, A. (2006) Coordinated effects of distal mutations on environmentally coupled tunneling in dihydrofolate reductase. *Proc. Natl. Acad. Sci. U.S.A. 103*, 15753–15758.
25. Warshel, A. (1991) Computer Modeling of Chemical Reactions in Enzymes, Wiley, New York.

26. Case, D. A., Cheatham, T. E., III, Darden, T., Gohlke, H., Luo, R., Merz, K. M., Jr., Onufriev, A., Simmerling, C., Wang, B., and Woods, R. J. (2005) The Amber biomolecular simulation programs. *J. Comput. Chem. 26*, 1668–1688.
27. Agarwal, P. K., Geist, A., and Gorin, A. (2004) Protein dynamics and enzymatic catalysis: Investigating the peptidyl-prolyl cis-trans isomerization activity of cyclophilin A. *Biochemistry 43*, 10605–10618.
28. Reece, L. J., Nichols, R., Ogden, R. C., and Howell, E. E. (1991) Construction of a synthetic gene for an R-plasmid-encoded dihydrofolate reductase and studies on the role of the N-terminus in the protein. *Biochemistry 30*, 10895–10904.
29. Beahm, R. (2007) Using molecular dynamics simulations to study the dynamics and catalytic properties of R67 DHFR. M.S. Thesis, University of Tennessee, Knoxville, TN.
30. Chemical Computing Group MOE, Molecular Operating Environment; Chemical Computing Group, Montreal.
31. Warshel, A. (2003) Computer simulations of enzyme catalysis: Methods, progress, and insights. *Annu. Rev. Biophys. Biomol. Struct. 32*, 425–443.
32. Pu, J., Ma, S., Garcia-Viloca, M., Gao, J., Truhlar, D. G., and Kohen, A. (2005) Nonperfect synchronization of reaction center rehybridization in the transition state of the hydride transfer catalyzed by dihydrofolate reductase. *J. Am. Chem. Soc. 127*, 14879–14886.
33. Cummins, P. L., and Gready, J. E. (2001) Energetically most likely substrate and active-site protonation sites and pathways in the catalytic mechanism of dihydrofolate reductase. *J. Am. Chem. Soc. 123*, 3418–3428.
34. Chopra, S., Lynch, R., Kim, S. H., Jackson, M., and Howell, E. E. (2006) Effects of temperature and viscosity on R67 dihydrofolate reductase catalysis. *Biochemistry 45*, 6596–6605.
35. Liu, H. B., and Warshel, A. (2007) The catalytic effect of dihydrofolate reductase and its mutants is determined by reorganization energies. *Biochemistry 46*, 6011–6025.
36. Nagel, Z. D., and Klinman, J. P. (2009) A 21(st) century revisionist's view at a turning point in enzymology. *Nat. Chem. Biol. 5*, 543–550.
37. Castillo, R., Andres, J., and Moliner, V. (1999) Catalytic Mechanism of Dihydrofolate Reductase Enzyme. A Combined Quantum-Mechanical/Molecular-Mechanical Characterizaton of Transition State Structure for the Hydride Transfer Step. *J. Am. Chem. Soc. 121*, 12140–12147.
38. Andres, J., Moliner, V., Safont, B. S., Domingo, L. R., Picher, M. T., and Krechl, J. (1996) On Transition Structures for Hydride Transfer Step: A Theoretical Study of the Reaction Catalyzed by Dihydrofolate Reductase Enzyme. *Bioorg. Chem. 24*, 10–18.
39. Desiraju, G. R., and Steiner, T. (1999) The weak hydrogen bond: In structural chemistry and biology, Oxford University Press, Oxford, U.K.
40. Billeter, S. R., Webb, S. P., Agarwal, P. K., Iordanov, T., and Hammes-Schiffer, S. (2001) Hydride transfer in liver alcohol dehydrogenase: Quantum dynamics, kinetic isotope effects, and role of enzyme motion. *J. Am. Chem. Soc. 123*, 11262–11272.
41. Almarsson, O., and Bruice, T. C. (1993) Evaluation of the Factors Influencing Reactivity and Stereospecificity in Nad(P)H Dependent Dehydrogenase Enzymes. *J. Am. Chem. Soc. 115*, 2125–2138.
42. Agarwal, P. K., Webb, S. P., and Hammes-Schiffer, S. (2000) Computational Studies of the Mechanism for Proton and Hydride Transfer in Liver Alcohol Dehydrogenase. *J. Am. Chem. Soc. 122*, 4803–4812.
43. Webb, S. P., Agarwal, P. K., and Hammes-Schiffer, S. (2000) Combining Electronic Structure Methods with the Calculation of Hydrogen Vibrational Wavefunctions: Application to Hydride Transfer in Liver Alcohol Dehydrogenase. *J. Phys. Chem. B 104*, 8884–8894.
44. Young, L., and Post, C. B. (1996) Catalysis by entropic guidance from enzymes. *Biochemistry 35*, 15129–15133.
45. Howell, E. E., Shukla, U., Hicks, S. N., Smiley, R. D., Kuhn, L. A., and Zavodszky, M. I. (2001) One site fits both: A model for the ternary complex of folate + NADPH in R67 dihydrofolate reductase, a D_2 symmetric enzyme. *J. Comput.-Aided Mol. Des. 15*, 1035–1052.
46. Deng, H., Callender, R., and Howell, E. (2001) Vibrational structure of dihydrofolate bound to R67 dihydrofolate reductase. *J. Biol. Chem. 276*, 48956–48960.
47. Hicks, S. N., Smiley, R. D., Hamilton, J. B., and Howell, E. E. (2003) Role of ionic interactions in ligand binding and catalysis of R67 dihydrofolate reductase. *Biochemistry 42*, 10569–10578.
48. Yahashiri, A., Nimrod, G., Ben-Tal, N., Howell, E. E., and Kohen, A. (2009) The effect of electrostatic shielding on H tunneling in R67 dihydrofolate reductase. *ChemBioChem 10*, 2620–2623.
49. Hicks, S. N., Smiley, R. D., Stinnett, L. G., Minor, K. H., and Howell, E. E. (2004) Role of Lys-32 residues in R67 dihydrofolate reductase probed by asymmetric mutations. *J. Biol. Chem. 279*, 46995–47002.
50. Feng, J., Goswami, S., and Howell, E. E. (2008) R67, the Other Dihydrofolate Reductase: Rational Design of an Alternate Active Site Configuration. *Biochemistry 47*, 555–565.
51. Richardson, J. S., and Richardson, D. C. (2002) Natural β-sheet proteins use negative design to avoid edge-to-edge aggregation. *Proc. Natl. Acad. Sci. U.S.A. 99*, 2754–2759.
52. Hellinga, H. (1998) Construction of a Blue Copper Analogue through Iterative Rational Protein Design Cycles Demonstrates Principles of Molecular Recognition in Metal Center Formation. *J. Am. Chem. Soc. 120*, 10055–10066.
53. Hecht, M. H., Richardson, J. S., Richardson, D. C., and Ogden, R. C. (1990) De novo design, expression, and characterization of Felix: A four-helix bundle protein of native-like sequence. *Science 249*, 884–891.